Corrosion-induced cover spalling and anchorage capacity

Corrosion-induced cover spalling and anchorage capacity

Kamyab Zandi[1,2]

[1]Department of Civil and Environmental Engineering
Chalmers University of Technology
412 96, Göteborg, Sweden

Material Group
[2]CBI Swedish Cement and Concrete Research Institute
501 15, Borås, Sweden

ABSTRACT

This study aims to enhance our understanding of anchorage capacity in reinforced concrete structures with corrosion-induced cover spalling. The objectives were to study the effect of high corrosion attacks leading to cover spalling through application of detailed numerical analysis, and to validate an existing one-dimensional (1D) analysis, based on one-dimensional bond-slip differential equation. Thus, earlier developed bond and corrosion models suited for detailed 3D finite element (FE) analysis were first combined with a new computational scheme to simulate corrosion-induced cover spalling. The 3D FE analysis and the 1D analysis were both validated with experiments. The application of 3D FE analysis to eccentric pull-out specimens showed that corrosion of stirrups advances the time to cracking and spalling, while the remaining bond strength is not significantly influenced by stirrup's corrosion. Moreover, it was shown that the magnitude of stresses in stirrups induced due to corrosion in the main bar highly depends on the spacing of main bar. Therefore, closely spaced main bars may cause large tensile stresses in stirrups which may need to be taken into account when shear capacity of RC structures is of concern.

Keywords: corrosion, reinforcement, deformed bar, cracking, cover spalling, bond-slip, anchorage, analytical model, numerical model,

1 Introduction

Infrastructures represent a large capital in all developed countries. To establish a sustainable development, it is of great importance that infrastructures generate a return and the investments result in safe structures with predictable response. Despite significant advances in construction design and practice, corrosion in reinforced concrete (RC) structures is still a leading cause of deterioration world-wide, Sustainable Bridges (2008). This has led to a growing concern for better assessment of existing concrete structures and revealed a need for improved understanding of the structural effects of corrosion.

Service life of reinforced concrete structures, according to the classical model of (Tuutti 1982), is divided into two phases: initiation and propagation. The initiation phase is defined as the period leading to depassivation of steel governed by the critical chloride concentration at the depth of the reinforcement (Silva 2013). Concerns about structural integrity of reinforced concrete arise during the propagation period when corrosion leads to a reduction in sectional area of reinforcing bars, (Almusallam 2001), (Cairns *et al.* 2005), and a change in the ductility of steel bars, (Du 2001), (Du *et al.* 2005). Furthermore, the volume expansion of corrosion products, that generates splitting stresses in the concrete, eventually cracks the surrounding concrete cover, (Andrade *et al.* 1993), (Rasheeduzzafar *et al.* 1992), (Molina *et al.* 1993), and adversely affect the bond between the reinforcement and concrete, (Al-Sulaimani *et al.* 1990), (Cabrera and Ghoddoussi 1992), (Clark and Saifullah 1993), (fib 2000), (Lundgren 2007), (Sæther 2009). For larger corrosion penetrations, the splitting stresses may lead to cover spalling, (Coronelli *et al.* 2011), which alters the resisting mechanism in the cross section, (Cairns and Zhao 1993), (Regan and Kennedy Reid 2009); stirrups then become the primary source of confinement (Zandi Hanjari 2010), see Figure 1. Therefore, the anchorage capacity of the structure is influenced by cover cracking (Lundgren 2007), cover spalling (Regan and Kennedy Reid 2009), as well as by the corrosion of stirrups (Higgins and Farrow III 2006) and (Regan and Kennedy Reid 2004). The structural behaviour of concrete structures with corrosion-induced cracking have been studied in several earlier works, (Zandi Hanjari *et al.* 2011d), (Coronelli and Gambarova 2004), (Rodriguez *et al.* 1995), (Almusallam *et al.* 1996), (Rodriguez *et al.* 1995), (Almusallam *et al.* 1996). However, the structural consequence of corrosion-induced cover spalling and of stirrups' corrosion is not yet fully understood; the former is the focus of the present study.

Cover spalling results in a decrease in the concrete cross-section and a loss of confinement. A reduction in the concrete cross-section leads to a decrease in the internal lever arm on the

compressive side, which in turn decreases the bending moment, (Rodriguez *et al.* 1997) and (Zandi Hanjari *et al.* 2011c). Loss of cover to, and full exposure of, tension reinforcement may change the structural behaviour from flexural to tied arch with secondary effects, (Cairns and Zhao 1993). Tests carried out on highly corroded beams with over 20% bar weight loss have shown that relatively high residual load-carrying capacity was reached when corroded beams failed in bending, see Azad et al. (2007), and Zhang (2008). Cover delamination may also reduce a member's resistance to shear cracking (Regan and Kennedy Reid 2010). Nevertheless, it is the impact of cover spalling on bond capacity and anchorage behaviour which, in most cases, is of the highest concern. (Regan and Kennedy Reid 2009) studied this by testing beams, cast without concrete cover, in which bars were either flush with the concrete surface or exposed to mid-barrel. A reduction of the bond strength up to 90% was observed for the bars exposed to mid-barrel; however, the volume expansion of rust and the effect of corroded stirrups were not taken into account. After all, the indicative values for the residual bond strength of corroded reinforcement given in Model Code 2010 (Zandi Hanjari 2006) covers only up to 5% corrosion weight loss, while the bond capacity for higher corrosion leading to cover spalling is still an open question. The present work is an effort in this direction.

This study aims to enhance our understanding of anchorage capacity in reinforced concrete structures with corrosion-induced cover spalling. The objectives of the work were (a) to study the effect of high corrosion attacks leading to cover spalling through application of detailed numerical analysis, and (b) to validate an existing one-dimensional (1D) analysis, based on one-dimensional bond-slip differential equation, for a case with corrosion-induced cover spalling. Thus, earlier developed bond and corrosion models suited for detailed 3D finite element (FE) analysis were first combined with a new computational scheme to simulate corrosion-induced cover spalling. The 3D FE analysis and the 1D analysis were both validated with two series of experiments and one empirical model available in the literature for anchorage capacity of corroded RC structures with cover spalling. The 3D FE analysis was then used to further investigate the influence of stirrups corrosion, corrosion distribution around a bar, and location of the bar at middle or corner positions of a concrete section.

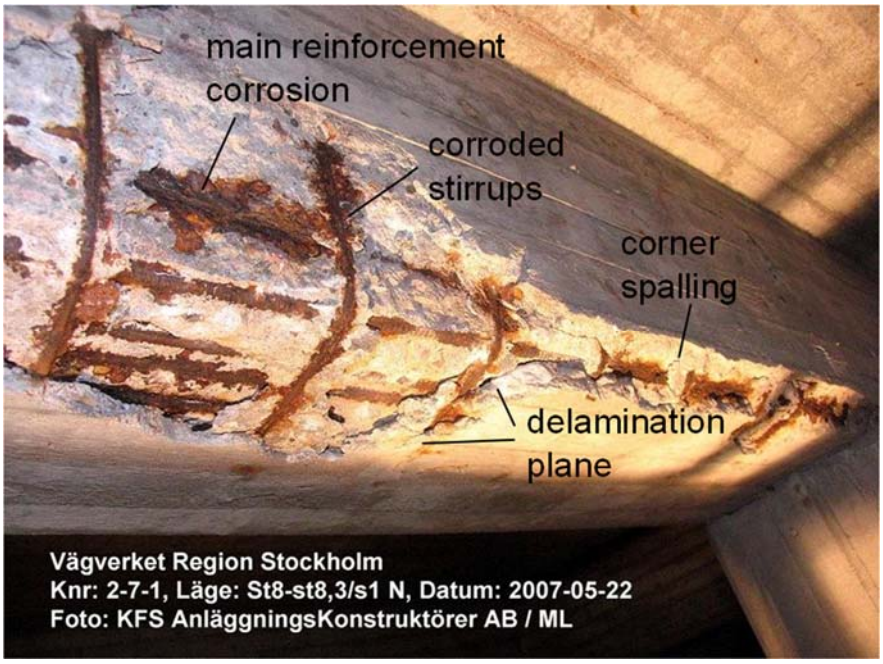

Figure 1. Delamination and corrosion of main bars and stirrups, Skurubron, Sweden; photo by Magnus Lindqvist.

2 Local bond-slip constitutive model after spalling

An analytical local bond-slip constitutive model for uncorroded reinforcement has been formulated in Model Code 1990 (CEB 1993). In an earlier work by (Lundgren *et al.* 2012a), the local bond-slip model in Model Code was extended to include corroded deformed bars. The bond-slip model for an uncorroded bar was first reformulated into a plasticity model. This allowed to conveniently incorporate corroded reinforcement, and made the model applicable for reversed and cyclic loading conditions. An interpolation scheme between the two extreme cases of "confined" and "unconfined", i.e. ductile pull-out failure and brittle splitting failure respectively, was proposed according to cover thickness and the amount of transverse reinforcement. Thereafter, based on the assumption that corrosion and anchorage action have a similar structural effect on surrounding concrete, as in both cases splitting stresses are induced, the bond-slip response of corroded reinforcement was obtained by shifting the bond-slip curve of uncorroded reinforcement along the slip axis. The extent to which the curve is shifted, ax, depends linearly on the corrosion penetration, see Figure 2. The model was earlier shown to give results that are on the safe side for cases when cover spalling has not taken place, (Lundgren *et al.* 2012a). However, the reflection of the model on cases with cover spalling had not been explored; this is studied in the following.

At cover spalling, the available confinement, $k_{spalling}$, to the reinforcement is correlated to the contribution of transverse reinforcement only as:

$$k_{spalling} = \left(\frac{f_{sw}}{\pi\tau_{max,con}}\right)\left(\frac{A_{sw}}{s\emptyset}\right) \leq 1 \quad (1)$$

where $k_{spalling}$ cannot be greater than 1.0.

Assuming "Good" bond conditions, the bond strength for "confined" and "unconfined" cases, based on Model Code 1990, are determined as in Equations (2) and (3), respectively.

$$\tau_{b,conf} = 0.40 \cdot \tau_{max,con} = 0.40 \cdot (2.5\sqrt{f_c}) = \sqrt{f_c} \quad (2)$$

$$\tau_{b,unconf} = 0.15 \cdot \tau_{max,uncon} = 0.15 \cdot (2.0\sqrt{f_c}) = 0.3 \cdot \sqrt{f_c} \quad (3)$$

Thereafter, the bond-slip relation is assumed to be the weighted sum of the bond-slip curves for "confined" and "unconfined" cases, according to

$$\tau_{b,spalling} = k_{spalling} \cdot \tau_{f,conf} + (1 - k_{spalling}) \cdot \tau_{f,unconf} \quad (4)$$

and that the bond strength at cover spalling for "Good" bond conditions is calculated as:

$$\tau_{b1,spalling} = \left(0.3 + \left(\frac{0.7 \cdot f_{sw}}{\pi\tau_{max,con}}\right)\left(\frac{A_{sw}}{s\emptyset}\right)\right) \cdot \sqrt{f_c} \quad (5)$$

where $0.3\sqrt{f_c} \leq \tau_{b1,spalling} \leq \sqrt{f_c}$; see Figure 2. Similarly, the bond strength at cover spalling for "All other" bond conditions is calculated as:

$$\tau_{b2,spalling} = \left(0.15 + \left(\frac{0.35 f_{sw}}{\pi\tau_{max,con}}\right)\left(\frac{A_{sw}}{s\emptyset}\right)\right) \cdot \sqrt{f_c} \quad (6)$$

where $0.15\sqrt{f_c} \leq \tau_{b2,spalling} \leq 0.5\sqrt{f_c}$.. The dimensionless function $\left(\frac{A_{sw}}{s\emptyset}\right)$ has also been used by (Regan and Kennedy Reid 2009) to relate the performance of a bent cantilever of stirrup providing restraint to the movement of the bar anchored in concrete. The function has been derived from test specimens in which the main bars were at the corners of stirrups. It has been recommended to assume $\left(\frac{A_{sw}}{s\emptyset}\right) = 0$ for bars, single or bundled, placed away from the corner of stirrups, and $\left(\frac{A_{sw}/2}{s\emptyset}\right)$ for bounded bars positioned at the corner of bent stirrups. These are advised to be adopted in Equations (5) and (6).

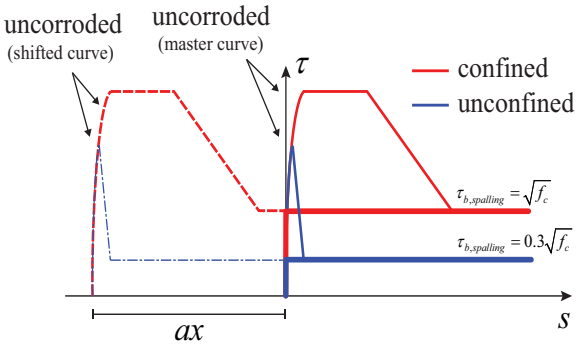

Figure 2. Local bond-slip reltion at cover spalling for "Good" bond conditions.

3 Empirical model for anchorage after spalling

Most empirical models for the anchorage of corroded bar are primarily concerned with relatively low corrosion attacks. To the author's knowledge, the only empirical model for the anchorage of bars with corrosion-induced cover spalling has been proposed by (Regan and Kennedy Reid 2009). The model is based on pull-out, beam, slab and splice tests carried out on specimens cast without cover to the main bars, which were either "flush" with the concrete surface or exposed to "mid-barrel". Regardless of the length of the bar embedded in concrete, the nominal bond stress (change of bar force per unit length divided by $\pi\emptyset$) is expressed as:

$$f_{b,flush} = (0.3 + 15\frac{A_{ss}}{s\emptyset})\sqrt{f_c} \leq 0.7\sqrt{f_c} \quad (7)$$

$$f_{b,mid-barrel} = (0.1 + 15\frac{A_{ss}}{s\emptyset})\sqrt{f_c} \leq 0.7\sqrt{f_c} \quad (8)$$

where the characteristic bond resistance specified in the British codes, $0.7\sqrt{f_c}$, has been chosen as the upper bound value. As mentioned before, the dimensionless function $\left(\frac{A_{sw}}{s\emptyset}\right)$ was used to express the stirrup restraint, where the effective stirrup area, A_{ss}, is suggested to be equal to the stirrup area, A_{sw}, for a single or bundled bar placed at the bent of a stirrup and equal to *zero* when it is placed away from the bent of the stirrups. Its extensions to other cases are justified to a greater or lesser extent in (Regan and Kennedy Reid 2009). It is important to note that the corrosion of stirrups, which is often severe at their bends and can cause loss of anchorage, is not counted for. The authors further clarify that the proposed bond stresses do not give characteristic values. They are however intended to be used in the analysis of beams and slabs for predictions of ultimate loads, which can reasonably be regarded as at a characteristic level, provided that the models in which they are used are in equilibrium and respect other relevant stress limits. A comparison of the bond strength after cover spalling based on the empirical

model of (Regan and Kennedy Reid 2009) and the analytical model of (Lundgren *et al.* 2012a) for varying transverse reinforcement contents and compressive strength is shown in Figure 3. The empirical model does not account for any additional confining effect for a transverse reinforcement content of higher than 0.04. The analytical model however relies on additional confining effect of transverse reinforcement even for $A_{sw}/s\phi$ higher than 0.04, provided that a "Good" bond condition is assumed. Overall, the prediction of the two models seems to highly depend on compressive strength as well as the choice of spalling pattern (flush and mid-barrel) and bond conditions ("Good" or "All other"). The models' predictions are later compared with experimental data and numerical simulations in section 5.2.

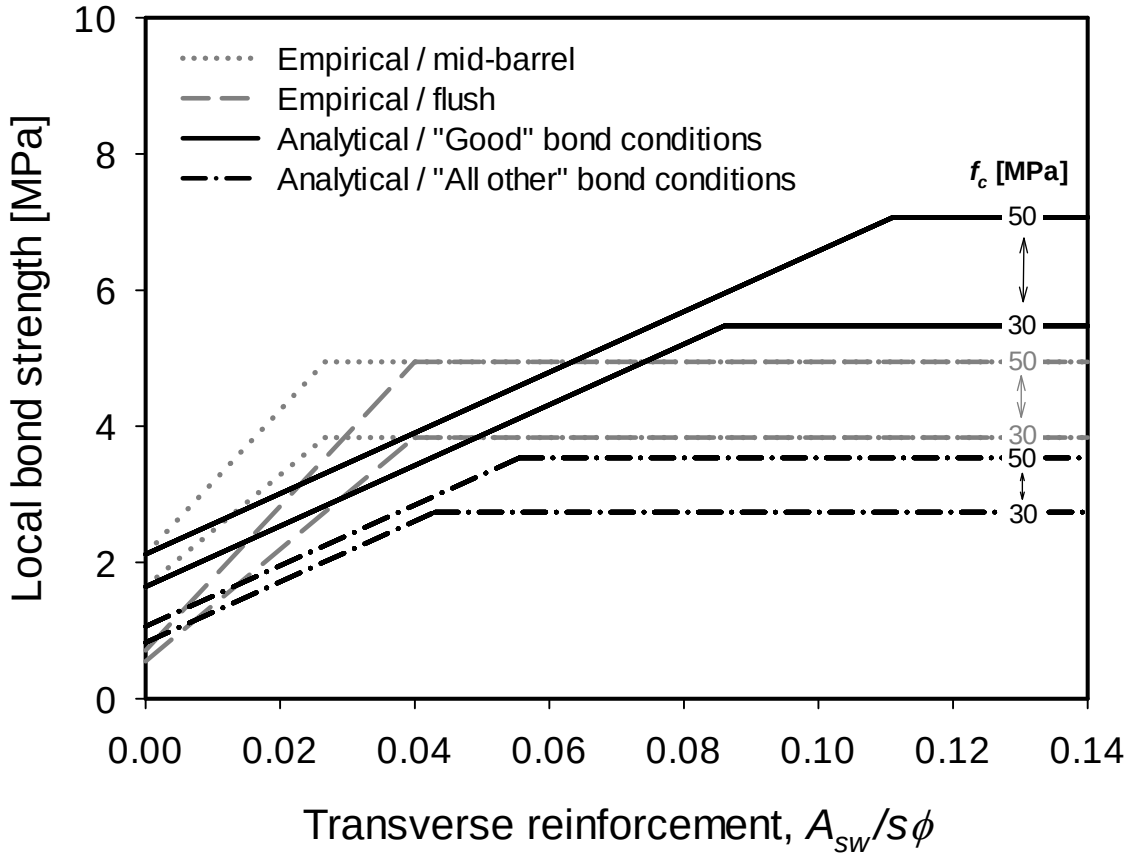

Figure 3. Comparison of the empirical and analytical models for bond strength after cover spalling by (Lundgren et al. 2012a) and (Regan and Kennedy Reid 2009), respectively.

4 Numerical modelling of anchorage, corrosion and spalling

The anchorage capacity of deformed bars in concrete is strongly influenced by the actual confinement conditions. In general, confinement is a result of the surrounding concrete, stirrups and transverse pressure. Corrosion of reinforcement leads to volume expansion of the steel,

which generates splitting stresses in the concrete; this influences the bond between the concrete and reinforcement. At a larger corrosion penetration, the splitting stresses may lead to cover cracking and, finally, spalling of the concrete cover. While corrosion of longitudinal reinforcement influences the bond and consequently the composite action, corrosion of stirrups weakens the confinement due to both the reduction in the stirrups' cross-sectional area and extensive cover cracking as a result of stirrups' corrosion. For a natural corrosive environment, in which both longitudinal and transverse reinforcements are corroded, anchorage and shear failures become more probable. These effects can be included in the analysis of reinforced concrete members with corrosion-induced cover spalling using different approaches with varying degrees of details, which are described in the following.

4.1 One-dimensional (1D) analysis

The anchorage length needed to anchor the yield force of a bar embedded in concrete can be calculated from a local bond-slip constitutive model, such as the one described in session 2, using the one-dimensional bond-slip differential equation (Lundgren *et al.* 2012b). If the bond-slip constitutive model is non-linear, the one-dimensional differential equation is also non-linear and needs to be solved numerically; such an analysis is referred to as 1D analysis in this paper. The equilibrium equation along a reinforcement bar is

$$\frac{\pi \cdot d^2}{4} \cdot \frac{d\sigma}{dx} - \pi \cdot d \cdot \tau = 0 \qquad (9)$$

where d is the rebar diameter, σ is the stress in the rebar and τ is the bond stress. The stress in the reinforcement is assumed to be in the elastic range according to

$$\sigma = E\varepsilon, \qquad \varepsilon = \frac{du}{dx} \qquad (10,11)$$

where E is the Young's modulus, ε is the strain and u is the displacement of the bar. The bond stress is here assumed to follow an elasto-plastic law

$$\tau = D(s - s_p), \qquad |\tau| \leq \tau_b(\kappa) \qquad (12,13)$$

where D is the bond stiffness, s is the slip, s_p is the plastic slip, and τ_b is the bond strength, which is a function of the hardening parameter κ. If deformation of the surrounding concrete is assumed to be negligible, the displacement of the bar becomes equal to the slip ($u = s$). The boundary conditions for the problem of pull-out of a bar with length L and a prescribed displacement u_L are:

$$\sigma_{(0)} = 0, \quad u_{(L)} = u_L \qquad (14,15)$$

The solution of the differential equation gives the deformation (slip) and stress along the bar as well as the pull-out force.

4.2 Two-dimensional (2D) FE analysis

Today, nonlinear structural analyses with two-dimensional solid (continuum) elements are the most common approach to model corroded reinforced concrete structures with the finite element method. In such models, the interaction between reinforcement bars and surrounding concrete is usually modelled with a bond-slip relation. The effect of corrosion is then introduced by adapting the local bond-slip constitutive model with respect to corrosion (Coronelli and Gambarova 2004) and (Zandi Hanjari *et al.* 2011b). The anchorage capacity calculated with 2D FE analysis is comparable to that calculated with 1D analysis if they both incorporate the same local bond-slip constitutive model such as the one in session 2. In both modelling approaches, the primary effect of corrosion, i.e. area reduction and ductility change of the reinforcement bars, can be taken into account.

One benefit with 2D FE analysis is the possibility to describe other modes of failure such as shear and bending in, for instance, a beam configuration, as well as their interaction with the anchorage action. Another advantage is that the available anchorage length is the output of 2D FE analysis; whereas, this needs to be known in advance in 1D analysis. However, the volume expansion of the corrosion products that generate splitting stresses in the concrete and leads to cracking and spalling cannot be directly accounted for in neither of approaches. A disadvantage of using a predefined bond-slip constitutive model as input for analysis is that several conditions must be known in advance, e.g. whether to assume “Good” or “All other” bond conditions, or how the corrosion of stirrups may influence the results. Therefore, more detailed modelling of the surrounding concrete and stirrups is required when large corrosion penetrations lead to extensive cover cracking and spalling, and when stirrups are subjected to corrosion. Such detailed analyses, validated with experiments, can form a firm foundation base on which bond-slip constitutive models can be calibrated for extreme cases.

4.3 Three-dimensional (3D) FE analysis

Three-dimensional finite element modelling has proved to be capable of describing the behaviour of reinforced concrete in a comprehensive way, provided that appropriate constitutive models are adapted. Furthermore, the effect of corrosion on the reinforcement, on the surrounding concrete and on their interaction can be simulated more realistically. Although

detailed structural analyses are numerically expensive, they allow for a more accurate description of the corrosion damage at the material and structural levels. Volume expansion of corrosion products, that leads to cover cracking and spalling, significantly influences the confinement conditions and consequently the steel/concrete bond. These effects have been taken into account in bond and corrosion models previously developed by (Lundgren 2005a), and (Lundgren 2005b), and extended by (Zandi Hanjari *et al.* 2013). In this work, these models were combined with a computation scheme to simulate the effect of corrosion-induced cover spalling on anchorage capacity. A short overview of the earlier developments of the model followed by the proposed computation scheme for corrosion-induced cover spalling is given below.

4.3.1 Overview of earlier developments of the model

In earlier work (Lundgren and Gylltoft 2000), a general model of the bond mechanism was developed; the model was later combined with the modelling of corrosion attack of reinforcement (Lundgren 2005a) and (Lundgren 2005b). The modelling approach is especially suited for detailed three-dimensional (3D) finite element analyses, where both concrete and reinforcement are modelled with solid elements, Figure 4 (a). Surface interface elements are used at the steel/concrete interaction to describe a relation between the stresses, σ, and the relative displacement, u, in the interface, Equations (16-18). The corrosion and bond models can be viewed as two separate layers around a reinforcement bar. Due to equilibrium between the two layers, the stress, σ, is the same in the bond and in the corrosion layers. The deformations in the bond and corrosion layers are solved in the interface element together with the condition for equilibrium using an iterative procedure, Equation (19).

The bond model, (Lundgren 2005a), is a frictional model describing the relations between stresses and deformations based on elasto-plastic theory, Figure 4 (b). The yield lines of the model are described by two yield functions: one describes the friction, F_1, assuming that the adhesion is negligible, and the other, F_2, describes the upper limit for a pull-out failure determined from the stress in the inclined compressive struts that result from the bond action, Equations (20-21). Consequently, the bond stress depends not only on the slip, but also on the radial deformation between the reinforcement bar and the concrete. Thus, the loss of bond at splitting failure or at yielding of reinforcement could be accounted for.

The corrosion model simulates the effect of corrosion as the volume increase of the corrosion products compared to the virgin steel (Lundgren 2005b), and accounts for the effect of corrosion products flowing through cracks (Zandi Hanjari *et al.* 2013). The volume of the

corrosion products relative to the uncorroded steel, υ_{rs}, the corrosion penetration depth into the steel bar as a function of the time, x, and the volume of corrosion products that flowed through a crack, V, are used to calculate the free increase of the bar radius, y_{ext}; see Figure 4 (c) and Equation (22). The corrosion time, i.e. duration of the corrosion process, and corrosion rate, i.e. corrosion penetration depth into the steel bar per unit of time, are inputs to the model and the corrosion penetration depth, x, is determined theoretically based on Faraday's law in Equations (23). The total strain in the corrosion products, ε_{cor}, is then calculated using Equation (24), and the corresponding stresses normal to the bar surface are determined from the normal strain in the corrosion products, Equation (25).

The volume of corrosion products that flows through a crack, V, is assumed to depend on the crack width and the normal stress in the corrosion products; see Figure 4 (d). The crack width closest to the bar, w_{cr}, is computed from the nodal displacements across the crack. It is assumed that the crack had a constant width of w_{cr} along its depth. The cross-sectional area of the crack through which corrosion products flows is then calculated as in Equation (26). A one-dimensional flow based on a plug flow model, i.e. constant velocity of the corrosion products flow along a crack, is applied to calculate the volume flow of corrosion products. The motion of the corrosion products is described with the Lagrangian formulation. The phenomenon is expressed as an ideal flow, i.e. the friction in the crack is assumed to be negligible. The motion of corrosion products particles is assumed to be driven by the normal stress in the corrosion products, σ_n, and thus the external force acting on the section area of the crack is calculated as in Equation (27). The amount of corrosion products transported across the section area of crack is then computed in time steps in Equation (28), and the total volume flow of corrosion products, V, through a crack in Equation (29).

(a) Implementation of bond and corrosion layers

$$\begin{bmatrix}\sigma_n\\ \sigma_t\\ \sigma_r\end{bmatrix}=\begin{bmatrix}D_{11} & 0 & 0\\ 0 & D_{22} & 0\\ 0 & 0 & D_{33}\end{bmatrix}\begin{bmatrix}u_n\\ u_t\\ u_r\end{bmatrix} \quad (16)$$

$$\sigma=\begin{bmatrix}\sigma_n\\ \sigma_t\end{bmatrix}=\begin{bmatrix}\text{normal stress}\\ \text{bond stress}\end{bmatrix} \quad (17)$$

$$u=\begin{bmatrix}u_n\\ u_t\end{bmatrix}=\begin{bmatrix}\text{relative normal displacement}\\ \text{slip}\end{bmatrix} \quad (18)$$

$$u_n=u_{ncor}+u_{nbond} \qquad u_t=u_{nbond} \qquad u_{tcor}=0 \quad (19)$$

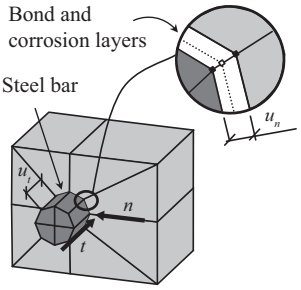

(b) Bond model in the bond layer

$$F_1=|\sigma_t|+\mu\sigma_n=0 \quad (20)$$

$$F_2=\sigma_t^2+\sigma_n^2+c\cdot\sigma_n=0 \quad (21)$$

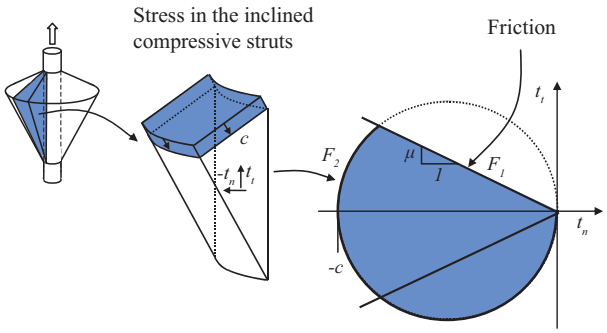

(c) Corrosion model in the corrosion layer

$$y_{ext}=-r+\sqrt{r^2+(\upsilon_{rs}-1)(2rx-x^2)-\frac{V}{\pi\cdot e}} \quad (22)$$

$$x=5.85\cdot(t\cdot I) \quad (23)$$

$$\varepsilon_{cor}=\frac{u_{ncor}-y_{ext}}{x+y_{ext}} \quad (24)$$

$$\sigma_n=K_{cor}\cdot\varepsilon_{cor}^{p} \quad (25)$$

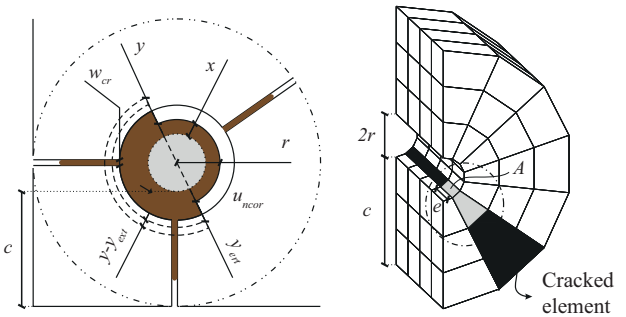

(d) Rust flow model in the corrosion layer

$$A_{cr}=A_1+A_2=w_{cr}\cdot e \quad (26)$$

$$\sum F=A_{cr}\cdot\sigma_n \quad (27)$$

$$\Delta V_i=\left[v_{i-1}+\frac{1}{2}\left(\frac{A_{cr,i-1}\cdot\sigma_{n,i-1}}{\rho(V_{i-1}+\Delta V_i)}\cdot\Delta t_i\right)\right]\cdot A_{cr,i-1}\cdot\Delta t_i \quad (28)$$

$$V=\sum_{i=1}^{k}\Delta V_i \quad (29)$$

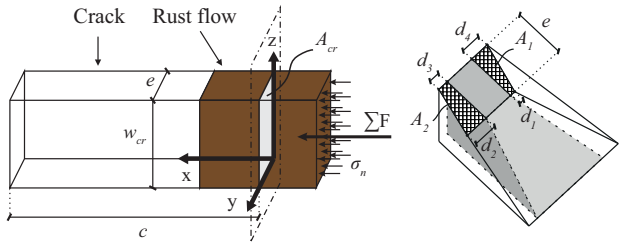

Figure 4. General overview of the model developments: (a) implementation of bond and corrosion layers (Lundgren 2005a), (b) bond model in the bond layer (Lundgren 2005a), (c) corrosion model in the corrosion layer (Zandi Hanjari et al. 2013), and (d) rust flow model in the corrosion layer (Zandi Hanjari et al. 2013).

4.3.2 Computation scheme for corrosion-induced cover spalling

Finite element analysis based on smeared crack formulations, including the rotating crack model, has difficulties in correctly representing geometrical discontinuity after the tensile softening of a finite element is completed. This results in a too stiff response at cracking due to spurious stress transfer, so-called stress locking, and spurious kinematic modes at spalling, so-called numerical instability, due to violation of displacement continuity assumption. A possibility to overcome stress locking in the smeared crack approach is to remove finite elements from the mesh as soon as their tensile softening is completed (Rots 1988). With this technique a gap propagates through the mesh behind the micro crack and the concrete at either side of the crack is elastically unloaded (Rots 1992). In this paper, a similar approach is adopted that allows possible changes in the topology of the mesh as corrosion-induced cracks connect and form a delamination plane.

A computation scheme for three-dimensional nonlinear FE analysis is devised which comprises several calculation phases. Each load step is applied in one calculation phase. In each phase a separate analysis is performed and the results from previous phases, typically stresses, are imposed as initial values. Between each phase a new finite element mesh is adapted excluding the elements that have completed their tensile softening and those that belong to delaminated part. However, these elements are excluded from the mesh only after a delamination plane is formed; in this respect the approach differs from that devised by (Rots 1992). This leads to a more stable analysis and enormous savings in computing time. Therefore, the poor kinematic representation of the discontinuous displacement field around a delamination plane after a full tensile softening is avoided. The computation scheme is outlined in Figure 5.

The examples provided in Figure 5 correspond to eccentric pull-out specimens which have the shape of a beam-end after inclined shear cracking, (Coronelli *et al.* 2013) and (Zandi Hanjari *et al.* 2011a). The two specimens differ with respect to the amount of longitudinal reinforcement; one with no stirrups along the embedment length (Type I) and the other with four stirrups along the embedment length (Type II). A detailed finite element analysis of these specimens, based on the approach summarized in section 4.3.1, is presented in (Zandi Hanjari *et al.* 2013). The analyses could only be carried out to a corrosion attack equivalent to rebar weight losses of around 10% and 15% for the specimen types I and II, respectively. These corrosion levels corresponded to extensive cover cracking, see Figure 5 (g) and (h). For higher corrosion attacks, the cracks connect and form a delamination plane and result in numerical instability in the analyses. However, the analyses with the proposed computation scheme could

be continued with larger corrosion penetration depths to compute corrosion-induced cover spalling as shown in Figure 5 (i) and (j). The difference in the spalling pattern in the two types of specimens is related to the amount of confinement. The analysis can thus be used to study the anchorage capacity of corroded specimens with cover spalling; this is an important advantage when the proposed computation scheme is used. In general, this scheme can be used to simulate geometrical discontinuity at cracking or spalling in any given stress state, as e.g. a splitting failure in a pull out test. However, in this paper the application of the computation scheme is validated only for corrosion-induced cover spalling. One drawback when using this approach is the prolonged computation time; therefore, it is recommended to use this in cases when the behaviour of a concrete member at or beyond cover spalling is of concern.

Without stirrups **With stirrups**

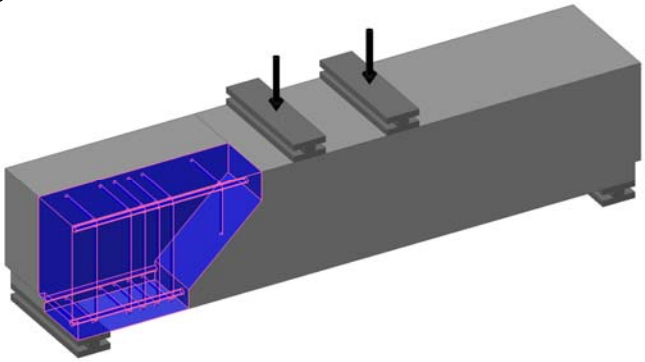

(a) Eccentric pull-out specimen in beam-end configuration

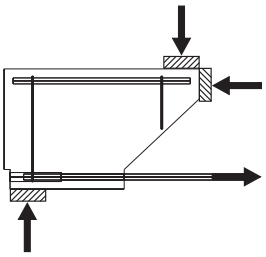

(b) Type I

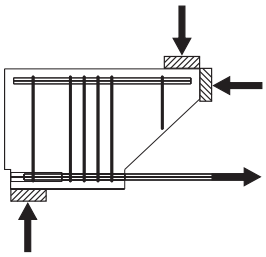

(c) Type II

FE Model adaptation for phase *m*

- Set-up a FE model
- Material properties is assigned (after adjustment if needed, e.g. E_c of corroded bar)
- BCs and loads are re-assigned
- Impose initial stresses $\sigma^0_{(m)} = \sigma_{(m-1)}$

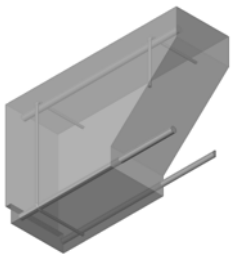

(e) Type I

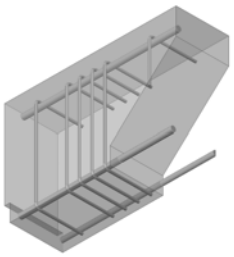

(f) Type II

Solving FE equations

- Load imposed in load steps

$$F_{(m)} + F_{\sigma^0_{(m)}} \xrightarrow{yields} \begin{cases} \Delta u_{(m)} \\ \Delta \varepsilon_{(m)} \\ \Delta \sigma_{(m)} \end{cases}$$

- Total results

$$u_{(m)} = u_{m-1} + \Delta u_{(m)} = u_{F_{(m)}} + u_{\sigma^0_{(m)}}$$
$$\varepsilon_{(m)} = \varepsilon_{(m-1)} + \Delta \varepsilon_{(m)}$$
$$\sigma_{(m)} = \sigma_{(m-1)} + \sigma^0_{(m)} + \Delta \sigma_{(m)}$$

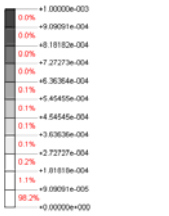

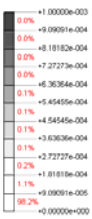

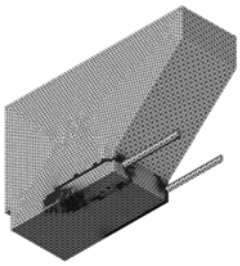

(g) Type I

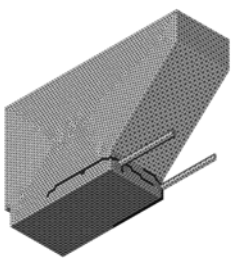

(h) Type II

Crack width evaluation

- Compute crack width

$$w_{cr} = 0.5 \sum_{node=1}^{4} u_{(m)_{node}}$$

if $w_{cr} \geq w_{cr,u}$

No

Yes

Evaluation of spalling pattern

- Remove the concrete elements which have completed their tensile softening
- Evaluate the delamination plane using element strains and nodal displacements
- Remove concrete elements that belong to delaminated/spalled cover
- Remove interface elements that share nodes with removed concrete elements

(d)

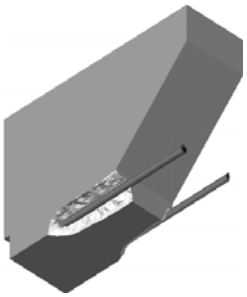

(i) Type I

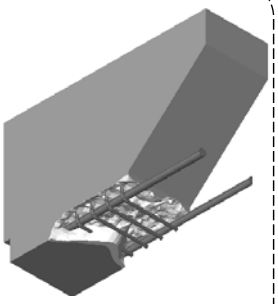

(j) Type II

Figure 5. Computation scheme to simulate corrosion-induced cover spalling, exemplified with eccentric put-out specimens by (Coronelli et al. 2013) and (Zandi Hanjari et al. 2011a).

5 Results and discussion of the analyses

5.1 One-dimensional (1D) analysis

The response of the 1D model to variations in stirrup's content, A_{sw}/ϕ, and cover-to-bar ratio, c/ϕ, is discussed here. To this aim, 1D analysis was applied to estimate the bond strength of eccentric pull-out specimens with dimensions of those tested by (Coronelli *et al.* 2013) and (Zandi Hanjari *et al.* 2011a). The results are shown in Figure 6 in terms of bond strength normalized with respect to the bond strength of a specimen with $c/\phi = 5$ and $A_{sw}/\phi = 0.05$ versus corrosion weight loss.

The importance of stirrup's content in delaying corrosion-induced bond deterioration can be recognized for varying corrosion levels at a constant cover-to-bar ratio of 1.5 in Figure 6. The confining effect of stirrups after cover cracking can particularly been seen at a relatively low corrosion level, $0\% \leq x_{cr} \leq 5\%$ associated to crack initiation phase. The contribution of concrete cover gradually decays with increased corrosion at an intermediate corrosion level of $5\% \leq x_{cr} \leq 30\%$, where the corrosion induced cracks propagate. At high corrosion levels, $x_{cr} \geq 30\%$ associate to cover spalling phase, the confining effect of concrete cover is fully exhausted and the bond capacity solely depends on stirrup's content and is calculated according to Equation (5).

The variation of bond strength in relation to varying concrete cover is shown in Figure 6 (b) and (c) at constant stirrup's contents of $A_{sw}/\phi = 0$ and 0.05 corresponding to specimen types I and II, respectively. In both cases, the bond strength strongly depends on the cover-to-bar ratio before cover cracking at $x_{cr} \leq 2\%$, and solely depends on the stirrup's content after cover cracking at $x_{cr} > 2\%$. For specimens without stirrups, the bond strength after cover cracking drops to a level that corresponds to bond strength at cover spalling. This is reasonable due to lack of the confining effect of stirrup. It should be noted that the increase in bond strength for a very low corrosion attack before cracking, commonly observed in experiments, owing to increased confinement due to expansion of corrosion products is not counted for in 1D analysis. Moreover, the interaction between adjacent bars is not included in these analyses either.

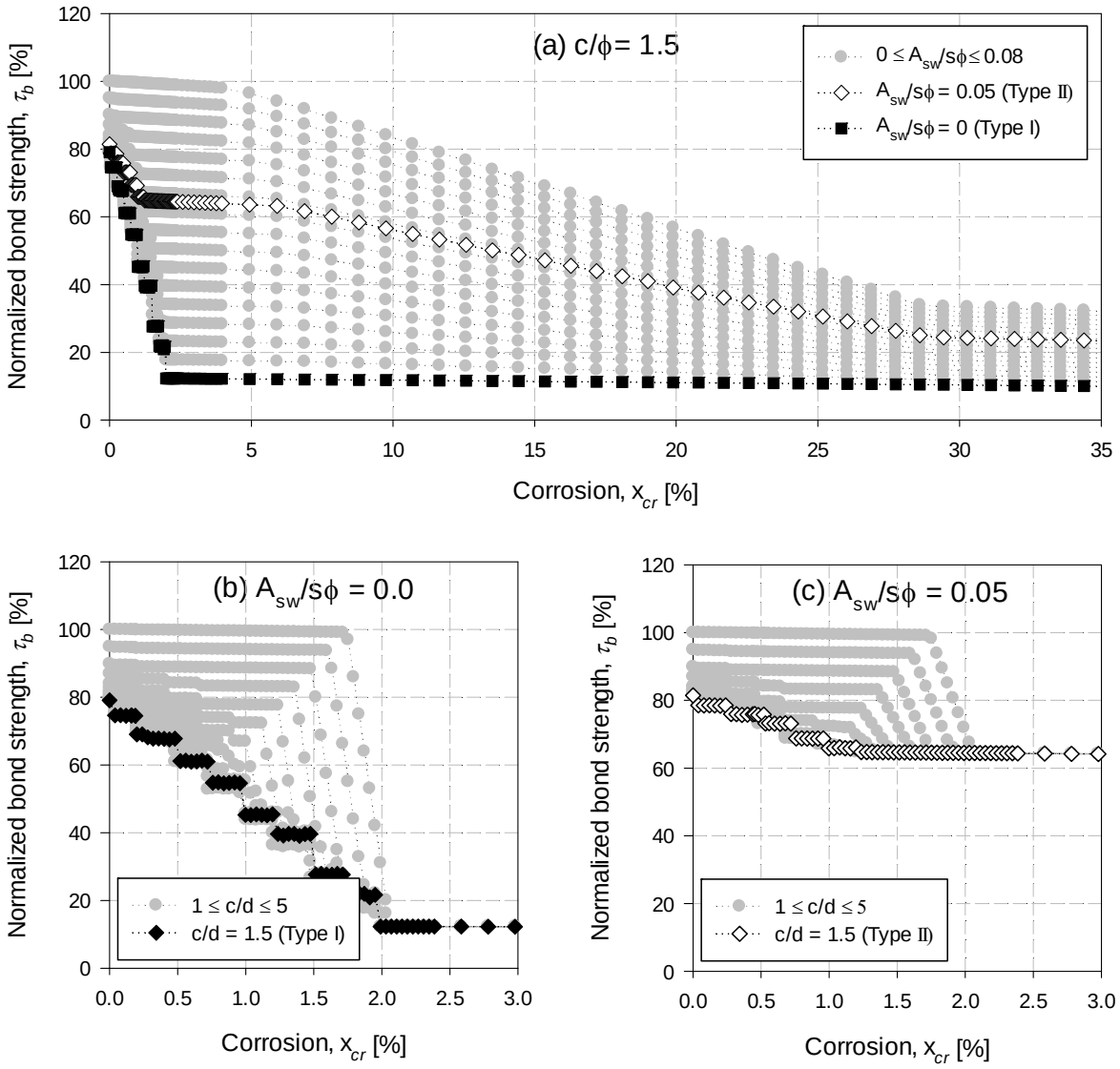

Figure 6. Bond strength of beam-end specimens estimated using 1D analysis with the assumption of "Good" bond conditions for (a) varying stirrups at c/ϕ = 1.5, (b) varying concrete cover at $A_{sw}/s\phi$ = 0.05 and (c) varying concrete cover at $A_{sw}/s\phi$ = 0.0; where l_b = 210 mm, ϕ = 20 mm, f_c = 28.7 MPa, E_s = 200 GPa, and *$f_y = f_{y,sw}$ = 510 MPa.*

5.2 Comparison of 1D and 3D analyses with experiments

The 1D analysis and 3D FE analyses were used to study three test series: the eccentric pull-out tests and beams with lap splices in region of constant moment by (Regan and Kennedy Reid 2009), and the eccentric pull-out tests by (Coronelli *et al.* 2013) and (Zandi Hanjari *et al.* 2011a). The test specimens are shown in Figure 7. The empirical model of Regan *et al.* for anchorage capacity after cover spalling is also evaluated with respect to the analyses and experiments. The 3D FE analyses were carried out in two phases. In the first phase, corrosion attack was applied in time steps as expansion of the corrosion products using the corrosion model, see Section 4.3.1. In the second phase, the bottom bar was pulled out using imposed displacement. An incremental static analysis was made using a Newton-Raphson iterative scheme to solve the non-linear equilibrium equations.

The eccentric pull-out tests by (Regan and Kennedy Reid 2009) were cast with three concrete covers of $c = 1.5\phi$ as "reference" specimen, $c = 0.5\phi$ in which the cover is "flush" with the concrete surface, and $c = 0$ where the cover is exposed to "mid-barrel". The results in terms of bond strength for varying transverse reinforcement contents are presented in Figure 8. These experiments were a part of the data base for which the empirical models in Equations 7 and 8 were calibrated; therefore, a good agreement is expected. The predictions based on empirical model as well as 1D and 3D FE analyses are also shown in Figure 8. The 1D analysis with "Good" bond conditions is on the safe side when compared with experimental data for flush and the corresponding empirical model. Whereas, the 1D analysis with "All other" bond conditions seems to be on the safe side only for a transverse reinforcement content higher than 0.01 when compared with experimental data for mid-barrel and the corresponding empirical model. The two spalling patterns, flush and mid-barrel, in the experimental data and empirical model as well as the two bond conditions, "Good" and "All other", in 1D analysis identify the extreme cases; whereas, an intermediate condition is most likely in reality based on field observations. This is best reflected with 3D FE analysis across all contents of transverse reinforcement.

The same three concrete covers as in the pull-out tests were also included in beam tests with splices in the region of constant moment by (Regan and Kennedy Reid 2009). The compressive strength of concrete varied slightly in the tests; that seems to be partly the reason for the scatter seen in Figure 9. The corresponding 1D analysis was therefore carried out with the highest and lowest compressive strength resulting in upper and lower limits, respectively. Similar to before,

it seems that the two spalling patterns of “flush” and “mid-barrel” are the two extremes, and that the 1D analysis makes safe predictions of bond strength at cover spalling.

The last series of experiment used here for comparison is the pull-out tests by (Coronelli *et al.* 2013) and (Zandi Hanjari *et al.* 2011a). As the level of corrosion in the experiments was not enough to result in cover spalling, these tests were only used for comparison of 1D and 3D FE analyses with the empirical model. The results are presented separately for the bond capacity of middle and corner bars in terms of normalized bond strength for varying transverse reinforcement contents in Figure 10. In case of a bar located in a corner position, the estimation based on 1D analysis remains between the empirical models for “flush” and “mid-barrel” for a relatively low transverse reinforcement content, and on the safe side with a reasonable margin for a high transverse reinforcement content. The 3D FE analysis show a slightly higher bond capacity in comparison with 1D analysis and empirical models for most transverse reinforcement content. All these observations also hold true for a bar located in a middle position. Overall, it is important to note that for a case with no transverse reinforcement the remaining bond capacity may be as small as 5 to 20%, however, the upper limit to this range can rapidly increase to above 30% in the presence of transverse reinforcement with $A_{sw}/\phi >$ 0.02. The test specimens were used for

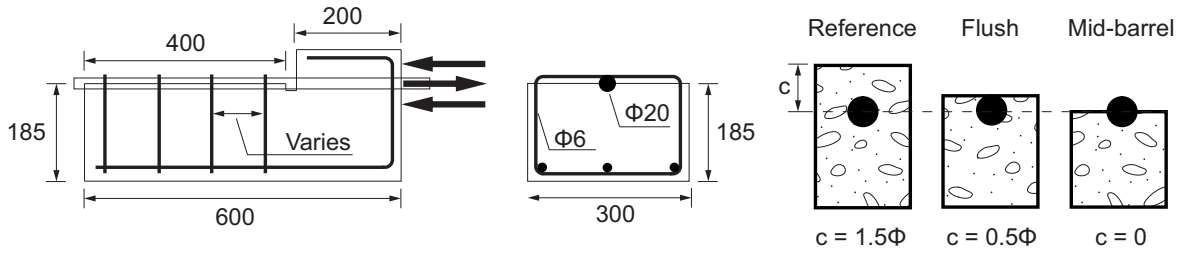

(a) Eccentric pull-out tests by (Regan and Kennedy Reid 2009)

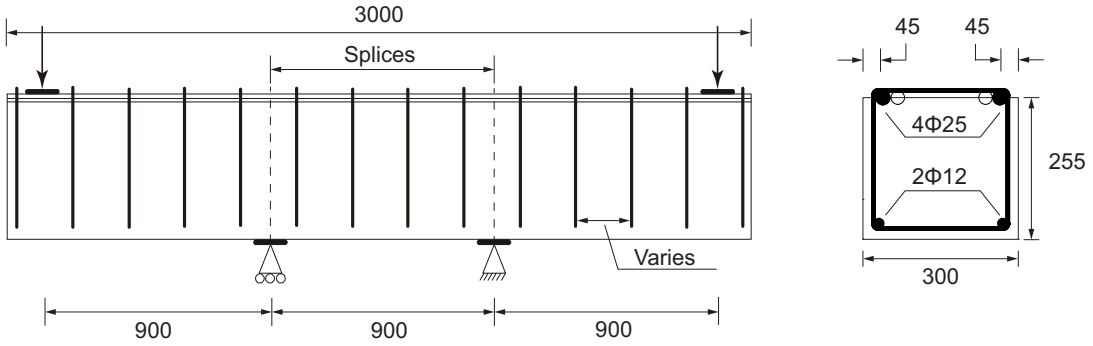

(b) Beams tests with lap splices by (Regan and Kennedy Reid 2009)

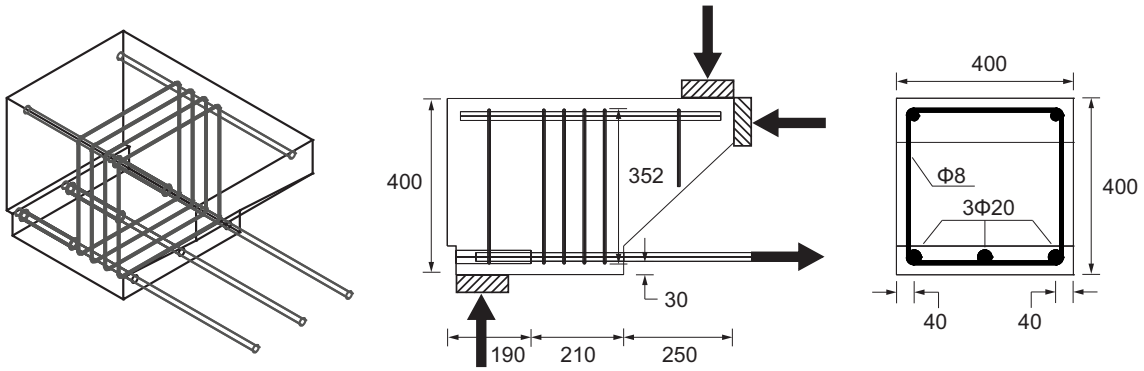

(c) Eccentric pull-out tests by (Coronelli et al. 2013) and (Zandi Hanjari et al. 2011a)

Figure 7. Test specimens and set-ups, all dimensions are in mm.

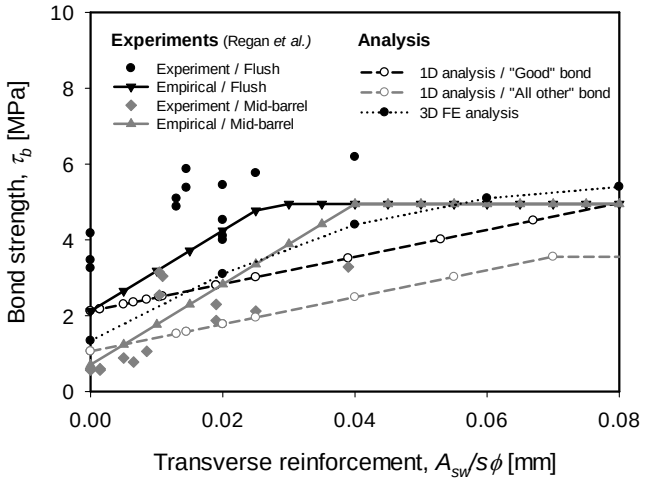

Figure 8. Analysis of eccentric pull-out tests by (Regan and Kennedy Reid 2009) for varying transverse reinforcement contents.

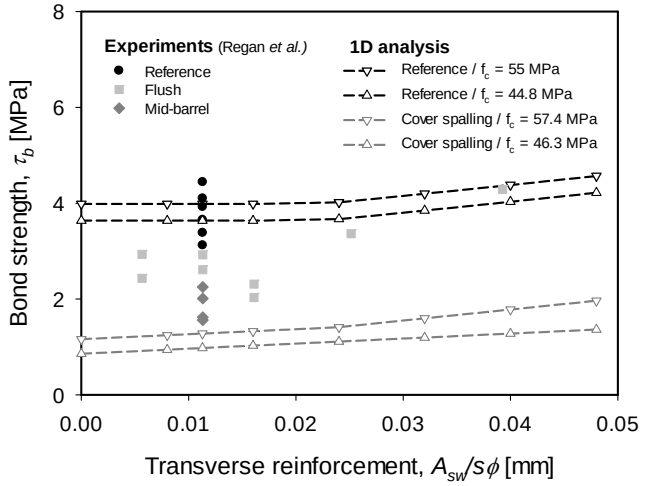

Figure 9. Analysis of beams with lap splices in region of constant moment tests by (Regan and Kennedy Reid 2009) for varying transverse reinforcement contents.

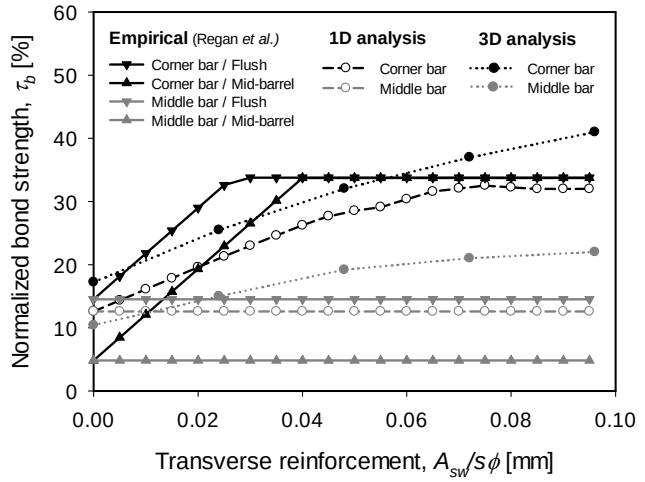

Figure 10. Analysis of eccentric pull-out tests by (Coronelli et al. 2013) and (Zandi Hanjari et al. 2011a) for varying transverse reinforcement contents.

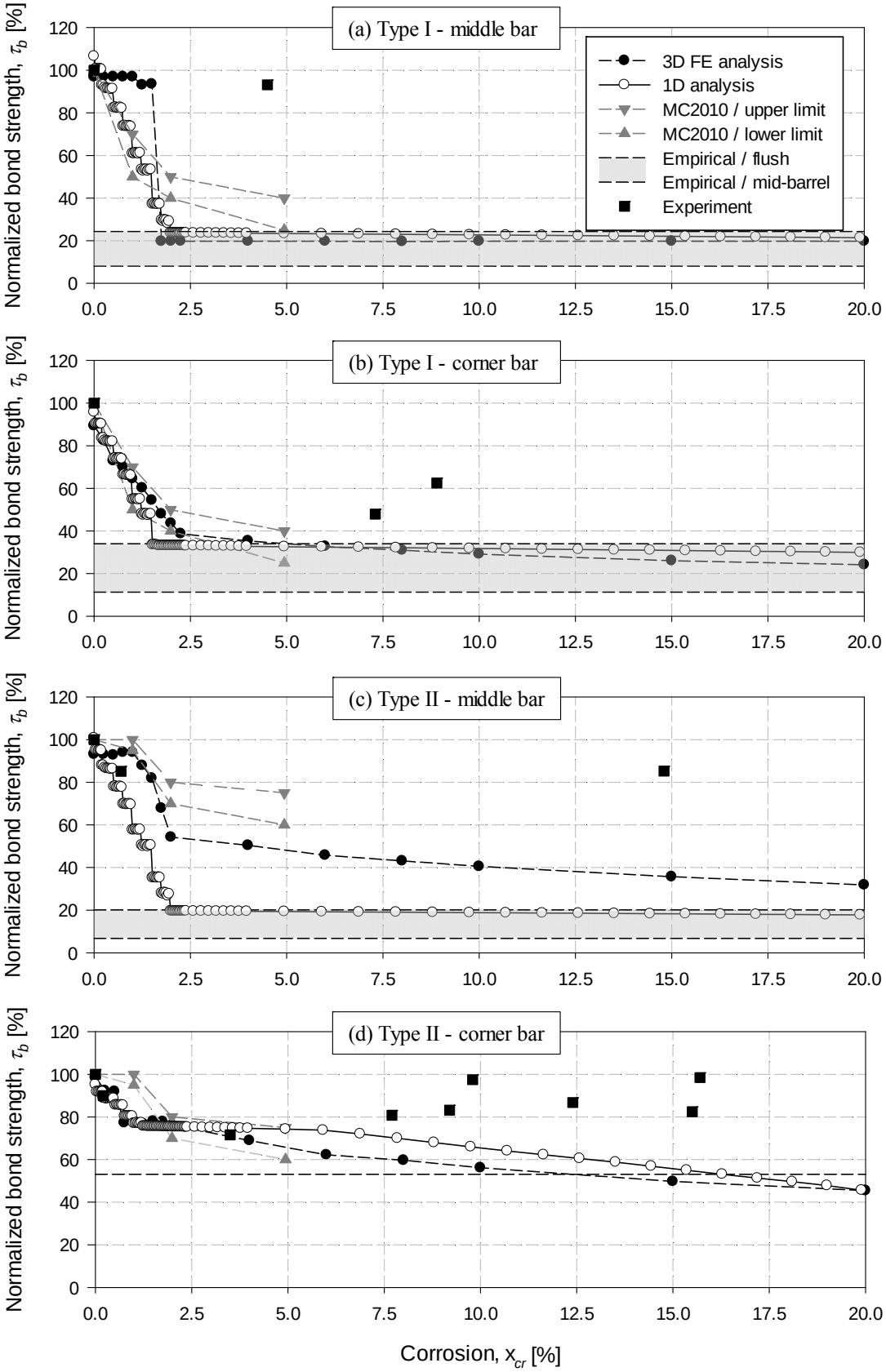

Figure 11. Detailed analysis of eccentric pull-out tests by (Coronelli et al. 2013) and (Zandi Hanjari et al. 2011a) for varying corrosion levels.

6 Application of the models

6.1 Influence of corrosion pattern around a bar

Most structures that are exposed to aggressive environment show that the steel bars are corroded non-uniformly. This is partly because the concrete cover to the surface of the bar varies all around the bar. More importantly, the corrosive environment surrounding the structure also varies which causes different corrosion pattern on the surface of a steel bar. The influence of varying corrosion pattern around a bar on the bond strength was investigated using 3D FE analysis of eccentric pull-out specimens tested by (Coronelli *et al.* 2013) and (Zandi Hanjari *et al.* 2011a). Four corrosion patterns were investigated where full, three quarter, half and one quarter of the bar's surface area was exposed to corrosion. Independent of the corrosion pattern around a bar, the same level of corrosion weight loss was imposed at a given section in all studied cases. The results of 3D FE analysis in terms of normalized bond strength for varying corrosion level are shown in Figure 12. This indicates that the bond strength in all cases is not significantly influenced by corrosion pattern. This observation seems to be valid for all cases with the same amount of corrosion weight loss; this is because the same pressure is introduced around the bar and that leads to the same bond loss.

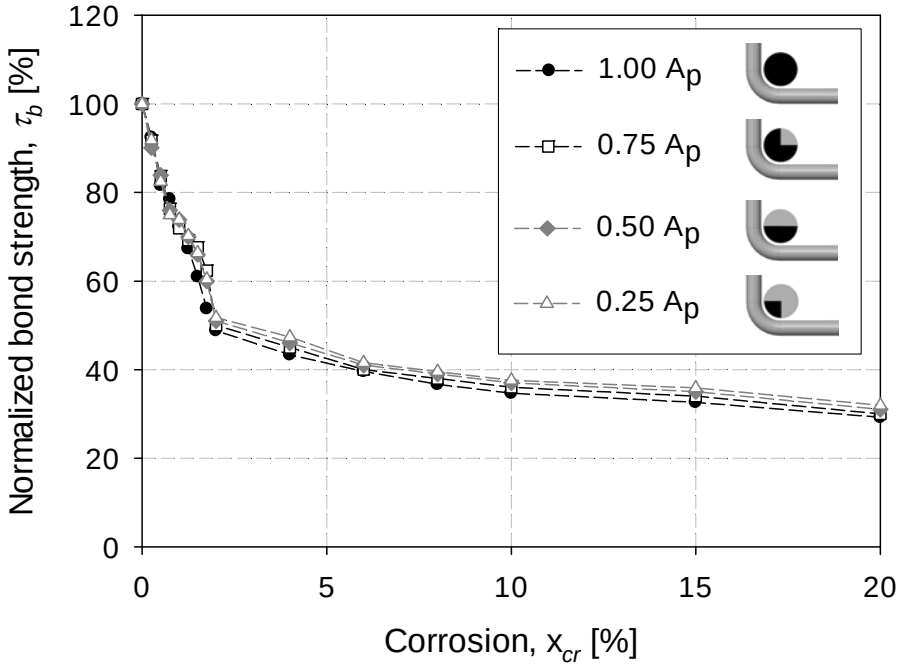

Figure 12. The influence of corrosion pattern around a bar on the bond strength, based on 3D FE analysis of eccentric pull-out specimens by (Coronelli et al. 2013) and (Zandi Hanjari et al. 2011a).

6.2 Effects of corroded stirrups

A rather common approach in modelling the effect of the corroded stirrups is to take into account the loss of the cross-sectional area; this does not account for the volume expansion of rust around the corroded stirrups, which may lead to cover cracking. Field investigations and laboratory tests have shown that cover delamination is more probable in areas with corroded stirrups, particularly when the stirrups are closely spaced (Higgins and Farrow III 2006). The effect of corrosion in stirrups was studied using 3D FE analysis of eccentric pull-out specimens tested by (Coronelli *et al.* 2013) and (Zandi Hanjari *et al.* 2011a).

The results in terms of normalized bond strength for varying corrosion level are shown in Figure 13 for three test specimens: with no stirrups along the embedment length (Type I), with four non-corroded stirrups along the embedment length (Type II), and with four corroding stirrups along the embedment length (Type III). The stirrup was modelled with three-dimensional solid elements, which enabled modelling of the corrosion of stirrups in the analyses. The results indicate that corrosion of stirrups advances the cracking in early stage of corrosion. Therefore, more bond strength is occurs at early stages; however, the same bond strength deterioration is observed after cover cracking. This seems to be true either when a corner bar or a middle bar is of concern; see Figure 13 (a) and (b), respectively.

This agrees with earlier observations. In an experimental program carried out by Higgins and Farrow III (2006), the shear capacity of beams with corroded stirrups was studied. An electrochemical method was used to produce corrosion in stirrups; corrosion of the flexural reinforcement was prevented. Extensive cracking, partial delamination and staining, were observed for sectional losses of stirrups of 12%, 20% and 40%. These authors showed that when stirrups were subjected to corrosion, spacing of the stirrups governed the extent of damage to the concrete cover. In regions with tightly spaced stirrups, the cover cracks from neighbouring stirrups interacted and caused larger areas of spalling and delamination. When stirrups were widely spaced, the damage to the concrete cover was more localized. It has also been shown that the capacity of the beams was reduced by up to 50% when the stirrups were highly corroded.

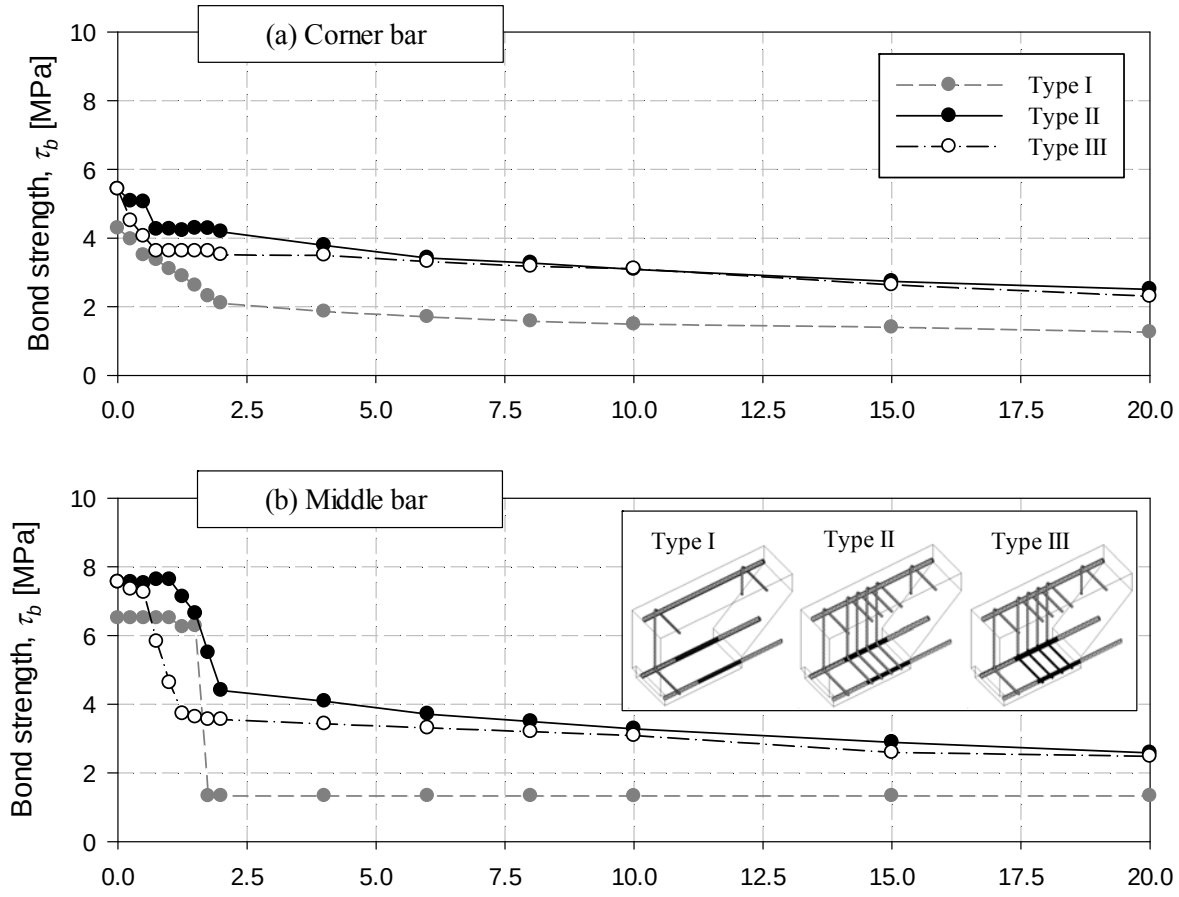

Figure 13. The influence of corrosion of stirrups on the bond strength, based on 3D FE analysis of eccentric pull-out specimens by (Coronelli et al. 2013) and (Zandi Hanjari et al. 2011a).

6.3 Effect of corrosion on the stress in transverse reinforcement

The expansion that takes place around corroded bars may results in tensile force not only in the surrounding concrete but also in the surrounding stirrups. If the magnitude of the induced stress in the stirrups becomes significant, it may lead to compromising the shear capacity of an RC member. The effect of corrosion of main bar on the stress in transverse reinforcement was studied using 3D FE analysis of eccentric pull-out specimens tested by (Coronelli *et al.* 2013) and (Zandi Hanjari *et al.* 2011a). The variation of stresses in stirrups due to 2, 5, 10 and 20% corrosion in the main bars are shown in Figure 14. This is shown for two cross-sections, one in which there are two corroding bars on the bottom, Figure 14 (a), and another in which there are three corroding bars on the bottom and one corroding bar on the top of the concrete cross-section, Figure 14 (b). The results show that the stresses in the stirrups may be as large as 80 MPa. Moreover, it can be seen that depending on the spacing between the main bars, there might be an increased stress in the stirrups due to the corrosion in the adjacent main bar. This agrees with earlier observation that indicates the important of main bar spacing in time to

cracking and spalling. Therefore, it can be concluded that the shear capacity of a corroded RC member may be influenced by corrosion, not only due to reduction of the cross-sectional area of corroded stirrups, but also due to induced stresses in stirrups as the results of corrosion in the main bars.

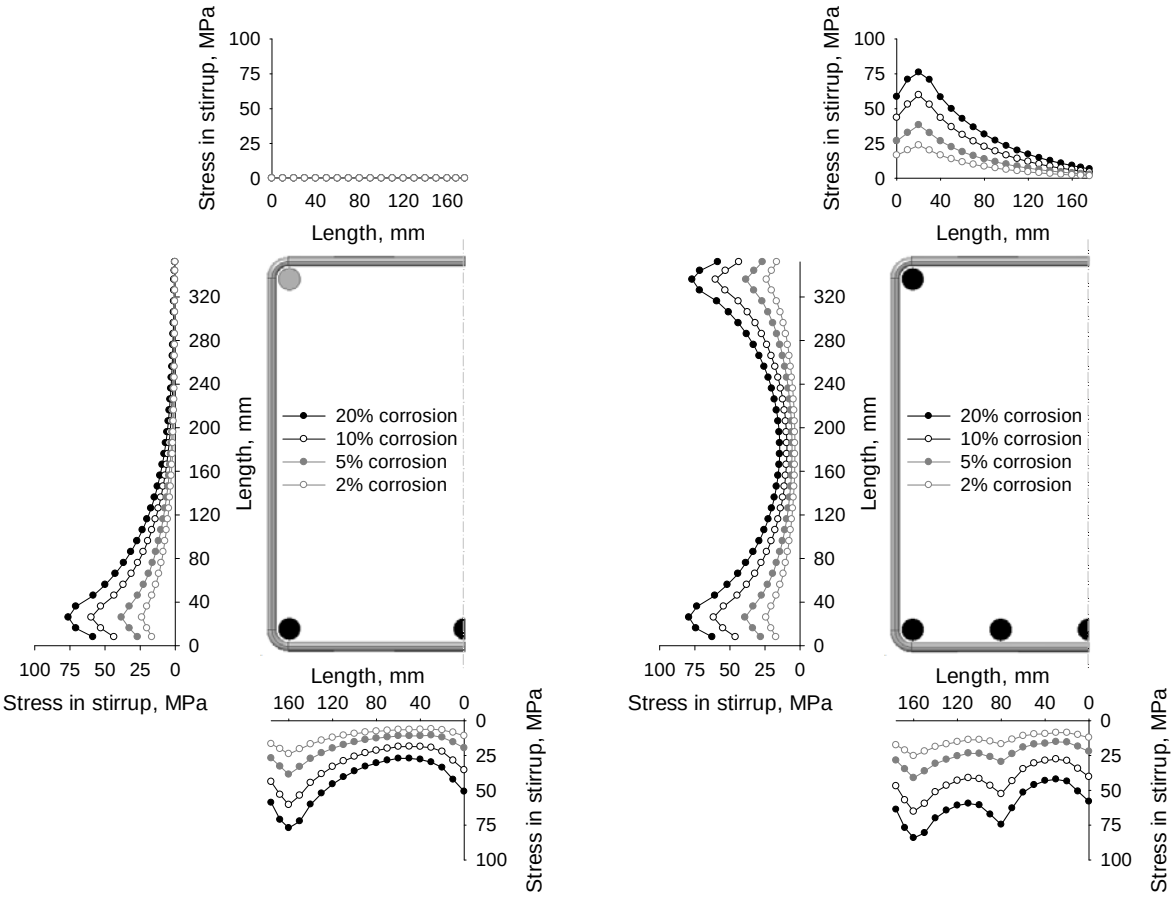

Figure 14. The influence of corrosion of main bar on the stress in stirrups, based on 3D FE analysis of eccentric pull-out specimens by (Coronelli et al. 2013) and (Zandi Hanjari et al. 2011a).

7 References

Al-Sulaimani, G.J., Kaleemullah, M., Basunbul, I.A. & Rasheeduzzafar, 1990. Influence of corrosion and cracking on bond behavior and strength of reinforced concrete members. *ACI Structural Journal,* 87 (2), 220-231.

Almusallam, A.A., 2001. Effect of degree of corrosion on the properties of reinforcing steel bars. *Construction and Building Materials,* 15 (8), 361-368.
Almusallam, A.A., Algahtani, A.S., Aziz, A.R., Dakhil, F.H. & Rasheeduzzafar, 1996. Effect of reinforcement corrosion on flexural behavior of concrete slabs. *Journal of Materials in Civil Engineering,* 8 (3), 123-127.
Andrade, C., Alonso, C. & Molina, F.J., 1993. Cover cracking as a function of bar corrosion.1. Experimental test. *Materials and Structures,* 26 (162), 453-464.
Cabrera, J.G. & Ghoddoussi, P., Year. The effect of reinforcement corrosion on the strength of the steel/concrete "bond"ed.^eds. *Bond in Concrete, Proceedings of an International Conference*, Riga: CEB, 10-11 - 10-24.
Cairns, J., Plizzari, G.A., Du, Y., Law, D.W. & Franzoni, C., 2005. Mechanical properties of corrosion-damaged reinforcement. *ACI Materials Journal,* 102 (4), 256-264.
Cairns, J. & Zhao, Z., 1993. Behaviour of concrete beams with exposed reinforcement. *Proceedings of the Institution of Civil Engineers, Structures and Buildings,* 99 (2), 141-154.
Ceb, 1993. *Ceb-fip model code 1990* Lausanne, Switzerland: Bulletin d'Information 213/214.
Clark, L.A. & Saifullah, M., 1993. Effect of corrosion on reinforcement bond strength. *In* Forde, M. ed. *5th international conference on structural faults and repairs.* Edinburgh: Engineering Technical Press, 113-119.
Coronelli, D. & Gambarova, P., 2004. Structural assessment of corroded reinforced concrete beams: Modeling guidelines. *Journal of Structural Engineering,* 130 (8), 1214.
Coronelli, D., Hanjari, K.Z., Lundgren, K. & Rossi, E., 2011. Severely corroded reinforced concrete with cover cracking: Part 1. Crack initiation and propagation. *In* Andrade, C. & Mancini, G. eds. *Modelling of corroding concrete structures.* 195-205.
Coronelli, D., Zandi Hanjari, K. & Lundgren, K., 2013. Severely corroded rc with cover cracking. *Journal of Structural Engineering-Asce,* 139 (2), 221-232.
Du, Y., 2001. *Effect of reinforcement corrosion on structural concrete ductility*. PhD thesis University of Birmingham, UK.
Du, Y.G., Clark, L.A. & Chan, A.H.C., 2005. Effect of corrosion on ductility of reinforcing bars. *Magazine of Concrete Research,* 57 (7), 407-419.
Fib, 2000. Bond of reinforcement in concrete, state-of-art report. Lausanne: Fédération internationale du béton, prepared by Task Group Bond Models, 427.
Higgins, C. & Farrow Iii, W.C., 2006. Tests of reinforced concrete beams with corrosion-damaged stirrups. *Aci Structural Journal,* 103 (1), 133-141.
Lundgren, K., 2005a. Bond between ribbed bars and concrete. Part 1: Modified model. *Magazine of Concrete Research,* 57 (7), 371-382.
Lundgren, K., 2005b. Bond between ribbed bars and concrete. Part 2: The effect of corrosion. *Magazine of Concrete Research,* 57 (7), 383-395.
Lundgren, K., 2007. Effect of corrosion on the bond between steel and concrete: An overview. *Magazine of Concrete Research,* 59 (6), 447-461.
Lundgren, K. & Gylltoft, K., 2000. A model for the bond between concrete and reinforcement. *Magazine of Concrete Research,* 52 (1), 53-63.
Lundgren, K., Kettil, P., Hanjari, K.Z., Schlune, H. & Roman, A.S.S., 2012a. Analytical model for the bond-slip behaviour of corroded ribbed reinforcement. *Structure and Infrastructure Engineering,* 8 (2), 157-169.
Lundgren, K., Kettil, P., Zandi Hanjari, K., Schlune, H. & San Roman, A.S., 2012b. Analytical model for the bond-slip behaviour of corroded ribbed reinforcement. *Structure & Infrastructure Engineering,* 8 (2), 157-169.
Molina, F.J., Alonso, C. & Andrade, C., 1993. Cover cracking as a function of rebar corrosion. 2. Numerical- model. *Materials and Structures,* 26 (163), 532-548.
Rasheeduzzafar, Al-Saadoun, S.S. & Al-Gahtani, A.S., 1992. Corrosion cracking in relation to bar diameter, cover, and concrete quality. *Journal of Materials in Civil Engineering,* 4 (4), 327-342.
Regan, P.E. & Kennedy Reid, I., 2004. Shear strength of rc beams with defective stirrup anchorages. *Magazine of Concrete Research,* 56 (3), 159-166.
Regan, P.E. & Kennedy Reid, I., 2009. Assessment of concrete structures affected by delamination: 1 - effect of bond loss. *Studies and Research - Annual Review of Structural Concrete,* 29, 245-275.

Regan, P.E. & Kennedy Reid, I., 2010. Assessment of concrete structures affected by delamination: 2 - bond-shear interaction. *Studies and Research - Annual Review of Structural Concrete,* 30, in press.

Rodriguez, J., Ortega, L.M. & Casal, J., 1995. The residual service life of reinforced concrete structures: Relation between corrosion and load bearing capacity of concrete beams. *The Residual Service Live of Reinforced Concrete Structures*. 33.

Rodriguez, J., Ortega, L.M. & Casal, J., 1997. Load carrying capacity of concrete structures with corroded reinforcement. *Construction and Building Materials,* 11 (4), 239-248.

Rots, J.G., 1988. *Computational modeling of concrete fracture*. Ph. D. thesis Delft University of Technology.

Rots, J.G., 1992. Removal of fnite elements in strain-softening analysis of tensile fracture. *In* Bazant, I.Z.P. ed. *Fracture Mechanics of Concrete Structures.* London and New York, 330-338.

Sæther, I., 2009. Bond deterioration of corroded steel bars in concrete. *Structure and Infrastructure Engineering, First published on: 29 July 2009 (iFirst), DOI: 10.1080/15732470802674836*.

Silva, N., 2013. *Chloride induced corrosion of reinforcement steel in concrete - threshold values and ion distributions at the concrete-steel interface*. (Doctoral thesis). Chalmers University of Technology.

Tuutti, K., 1982. *Corrosion of steel in concrete*: Swedish Cement and Concrete Research Institute.

Zandi Hanjari, K., 2006. *Evaluation of wst method as a fatigue test for plain and fiber-reinforced concrete - experimental and numerical investigation*. Chalmers tekniska högskola.

Zandi Hanjari, K., 2010. *Structural behaviour of deteriorated concrete structures*. (Doctoral). Chalmers University of Technology.

Zandi Hanjari, K., Coronelli, D. & Lundgren, K., 2011a. Bond capacity of severely corroded bars with corroded stirrups. *Magazine of Concrete Research,* 63 (12), 953-968.

Zandi Hanjari, K., Kettil, P. & Lundgren, K., 2011b. Analysis of mechanical behavior of corroded reinforced concrete structures. *ACI Structural Journal,* 108 (5), 532-541.

Zandi Hanjari, K., Lundgren, K., Plos, M. & Coronelli, D., 2013. Three-dimensional modelling of structural effects of corroding steel reinforcement in concrete. *Structure and Infrastructure Engineering,* 9 (7), 702-718.

Zandi Hanjari, K., Lundgren, K., Plos, M. & Gylltoft, K., 2011c. Corroded reinforced concrete structures: Effects of high corrosion and corroded stirrups. *Proceeding of XXI Nordic Concrete Research Symposium.* 179-182.

Zandi Hanjari, Z., Kettil, P. & Lundgren, K., 2011d. Analysis of mechanical behavior of corroded reinforced concrete structures. *Aci Structural Journal,* 108 (5), 532-541.